

## Article

# Energy Saving Performance of Agricultural Tractor Equipped with Mechanic-Electronic-Hydraulic Powertrain System

Zhen Zhu <sup>1</sup>, Yanpeng Yang <sup>2</sup>, Dongqing Wang <sup>2</sup>, Yingfeng Cai <sup>1</sup> and Longhui Lai <sup>1,\*</sup> 

<sup>1</sup> Automotive Engineering Research Institute, Jiangsu University, Zhenjiang 212013, China; 1000004750@ujs.edu.cn (Z.Z.); 1000004192@ujs.edu.cn (Y.C.)

<sup>2</sup> State Key Laboratory of Power System of Tractor, Luoyang 471039, China; yyp@ytjszx.com (Y.Y.); wdq@ytjszx.com (D.W.)

\* Correspondence: 2211904012@stmail.ujs.edu.cn; Tel.: +86-157-5101-8155

**Abstract:** Tractors are usually applied in field operations, road transport, and other operations. Modern agriculture has higher design requirements for tractor powertrains due to the complicated working environments and various operations. To meet the driving requirements of the tractor under multiple operations, a mechanic-electronic-hydraulic powertrain system (MEH-PS) for tractors has been designed according to the characteristics of the hydro-mechanical composite transmission and electromechanical hybrid system. The principle of multiple driven and transmission modes of MEH-PS are introduced, the speed regulation characteristic curve of hydro-mechanical transmission (HMT) is given, and the related power element model, tractor model, and efficiency model are established. The HMT optimal economy transmission ratio control strategy and hybrid rule-based optimization energy management strategy were developed. Take three typical tractor operations for analysis: ploughing, harvesting, and transport. The results show that the engine operating points are mainly distributed in the higher load area, the tractor maintains high system efficiency, and the relative error between simulated and tested fuel consumption is within 5%, which further proves the reliability of the model. The solution also showed lower fuel consumption in all three operations compared to DLG's announced PowerShift tractors and CVT tractors. Thus, the powertrain system can meet the tractor's drive requirements under complex operating conditions and maintain high efficiency and is therefore suitable for tractors that need to operate frequently in the field and on the road.



**Citation:** Zhu, Z.; Yang, Y.; Wang, D.; Cai, Y.; Lai, L. Energy Saving Performance of Agricultural Tractor Equipped with Mechanic-Electronic-Hydraulic Powertrain System. *Agriculture* **2022**, *12*, 436. <https://doi.org/10.3390/agriculture12030436>

Academic Editor: Francesco Marinello

Received: 28 February 2022

Accepted: 18 March 2022

Published: 21 March 2022

**Publisher's Note:** MDPI stays neutral with regard to jurisdictional claims in published maps and institutional affiliations.



**Copyright:** © 2022 by the authors. Licensee MDPI, Basel, Switzerland. This article is an open access article distributed under the terms and conditions of the Creative Commons Attribution (CC BY) license (<https://creativecommons.org/licenses/by/4.0/>).

**Keywords:** agriculture tractor; powertrain design; composite transmission; hybrid tractor; energy saving

## 1. Introduction

Tractors are extremely important in modern agriculture. According to the data issued by the Ministry of Agriculture and Rural Affairs, China's total number of various types of tractor surpassed 22.24 million by 2019, and the annual usage of agricultural diesel reached 2003 million tons, with a steady increasing trend [1]. China's 13th five-year plan for energy development and the 2022 Central Document No. 1 both aim to promote energy savings in agricultural production [2,3]. The higher the production efficiency, the higher the performance requirements of the tractor, reducing fuel consumption while improving tractor performance brings challenges to the design of tractor powertrains [4].

Hydrostatic transmission, mechanical transmission, and hydro-mechanical transmission are the most common transmission modes for tractors [5,6]. Hydrostatic transmission has the advantage of stepless transmission, but most tractors are not suitable for long operation of hydrostatic transmission to ensure transmission efficiency [7]. The operation of the mechanical transmission is complex, and for tractors with a wide range of power variations, more gears are required to meet the requirements of the corresponding operations [8], and ordinary gear transmission cannot realize stepless speed change [9]. Hydro-mechanical

transmission realizes stepless speed change by combining hydraulic and mechanical transmissions into a composite transmission that can meet the transmission requirements of a high-horsepower tractor while also ensuring the engine operates on the optimal economic curve by adjusting the transmission ratio [10]. Xiao studied the transmission ratio control strategy to maximize the engine and HMT overall efficiency [11]. Ahn proposed a control algorithm to realize the optimal economy of the tractor by controlling the transmission ratio of HMT [12]. The above study can indeed achieve fuel savings in the actual operation of the tractor. However, the hydraulic system is inefficient under part-load conditions due to volumetric efficiency [13]. When tractors perform the transit operation which is usually unloaded, it will lead to a decrease in tractor efficiency due to low load [14].

Electrification of road vehicles indicates that hybrid systems use battery energy to assist the engine to perform work at high loads, and use the remaining engine power to charge the battery at low loads, which can effectively reduce fuel consumption and improve vehicle performance, as well as for tractors [15,16]. Guo proposes a SOC-constraint-based energy management strategy, which was tested on a bus with a 5.9% fuel saving rate [17]. Kim found that hybrid tractors have a better economy than conventional tractors at part-load conditions due to the hybrid system regulating the engine operating point to an efficient region and turning off the engine for a purely electric drive when necessary [18,19]. A tractor starting with a load requires large torque because the electrical components' power density is much smaller than the hydraulic components, which requires high battery and motor power, resulting in large equipment size. Hydraulic components make up for this shortcoming and have the advantage of starting smoothly with better comfort [20]. Another significant difference between tractors and road vehicles is the need for additional power to the power take-off (PTO), and one of the key issues in modern tractor design includes the independence of the PTO output speed from the wheel speed [21].

In this study, a MEH-PS for tractors is proposed to solve the problems of conventional HMT and the hybrid system in tractors [22], which enables the tractor to have good driving performance and high efficiency from low to high load and from low to high speed. The hydro-electro-mechanical transmission (HEMT) was proposed by Haughery, who studied its transmission performance without considering the energy problem [23]. This paper first studies the structural principle of the MEH-PS and establishes the mathematical model of each component, then the ratio control strategy of HMT and the rule-based optimal energy management strategy of the hybrid system are developed. Finally, the scheme was simulated and tested in ploughing, harvesting, and transportation operations using SimulaitonX model and manufactured test bench successively, and compared with the fuel consumption of PowerShift tractors and CVT tractors published by DLG to verify the advantages of the powertrain compared with those of conventional tractors.

## 2. Principle of Powertrain Configuration

### 2.1. Driving Mode Analysis

A mechanic-electronic-hydraulic powertrain system with independent intellectual property rights was designed for tractors, and the main components are shown in Figure 1. The powertrain system consists of a diesel engine, an electric motor (EM), a set of power batteries, a variable displacement pump, a fixed displacement motor, four planetary gear mechanisms, three fixed shaft gears, five clutches, and five brakes. Where C1~C5 are clutches, B1~B5 are brakes, PG1~PG4 are planetary gears,  $i_1 \sim i_3$  are the transmission ratios of gear pairs, and  $e$  is the displacement ratio of the hydraulic system.

The powertrain system has two power sources, and the clutches C1, C2, and C3 and the brake B1 can be controlled to achieve four driving modes. Table 1 shows the switching element engagement states of each mode.

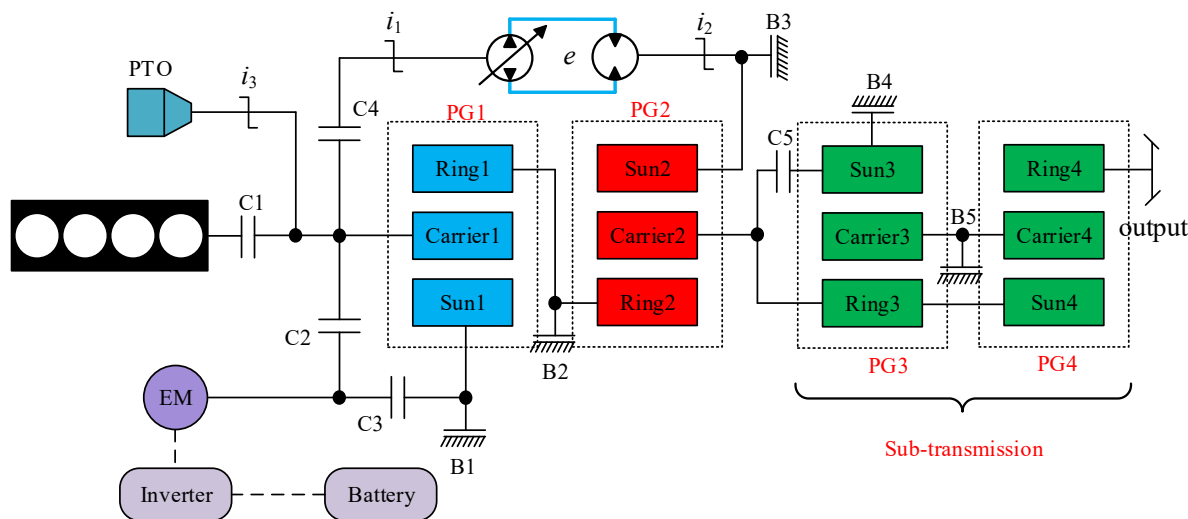


**Figure 1.** Configuration Scheme.

**Table 1.** Element engagement status of each driving mode.

Driving Mode	C1	C2	C3	B1
Pure electric drive (1)			▲	▲
Pure engine drive (2)	▲			▲
Torque coupling drive (3)	▲	▲		▲
Speed coupling drive (4)	▲		▲	

Note: “▲” means that the switching element is in the engaged state, the same is below.

## 2.2. Transmission Mode Analysis

There are three transmission modes of HMT. Hydrostatic transmission, hydro-mechanical transmission, and mechanical transmission can all be achieved by controlling clutches C4 and C5 and brakes B1, B2, B3, B4, and B5. Table 2 shows the transmission ratio and switching element engagement states of each mode.

**Table 2.** Element engagement status and transmission ratio of each gear.

Gear	C4	C5	B1	B2	B3	B4	B5	$i_g$
F(H)	▲			▲			▲	$\frac{i_1 i_2 k_4 (1+k_2)}{e}$
R(H1)	▲			▲		▲		$\frac{i_1 i_2 k_4 (1+k_2)(1+k_3)}{e(k_3 k_4 - 1)}$
R(H2)	▲	▲		▲				$\frac{i_1 i_2 (1+k_2)}{e}$
F (HM1)	▲			▲		▲		$\frac{i_1 i_2 k_1 k_4 (1+k_2)(1+k_3)}{[k_1 e + k_2 i_1 i_2 (1+k_1)](k_3 k_4 - 1)}$
F (HM2)	▲	▲	▲					$\frac{i_1 i_2 k_1 (1+k_2)}{k_1 e + k_2 i_1 i_2 (1+k_1)}$
R(HM)	▲		▲				▲	$\frac{k_1 k_4 (1+k_2)(1+k_3)}{k_2 (1+k_1)(k_3 k_4 - 1)}$
F (M1)			▲		▲	▲		$\frac{k_1 k_4 (1+k_2)(1+k_3)}{k_2 (1+k_1)(k_3 k_4 - 1)}$
F (M2)	▲	▲		▲				$\frac{k_1 (1+k_2)}{k_2 (1+k_1)}$
R(M)			▲		▲		▲	$\frac{-k_1 k_4 (1+k_2)}{k_2 (1+k_1)}$

Where F is forward gear, R is reverse gear, H is hydrostatic transmission, M is mechanical transmission, HM is hydro-mechanical transmission;  $i_g$  is the transmission ratio.

Keeping the speed of the tractor at mechanical gear as much as possible with the frequent speeds over the life cycle of the tractor can obtain a higher operating efficiency of the tractor. The parameters of each transmission element are obtained by a genetic algorithm, as shown in Table 3 [24].

**Table 3.** Transmission element parameters.

Parameters	$k_1$	$k_2$	$k_3$	$k_4$	$i_1$	$i_2$
Value	1.80	1.60	1.65	1.65	0.62	1.00

Where  $k_1 \sim k_4$  are the standing ratio of the planetary gears.

The above parameters are substituted into each transmission ratio to obtain the curve of transmission ratio about displacement ratio shown in Figure 2.

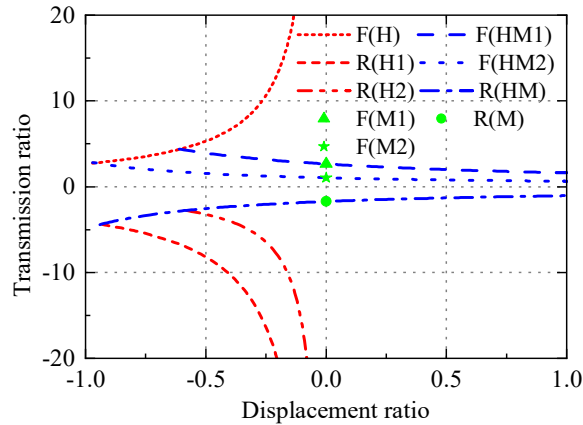


**Figure 2.** HMT speed regulation characteristic curve.

### 3. Powertrain Modeling

#### 3.1. Engine Model

The research object of this paper is a tractor, which is usually equipped with a diesel engine. The engine modeling is mostly a static model, which can reflect the engine characteristics within a certain accuracy. The static interpolation model of the engine can be established as follows [25]:

$$\begin{cases} T_e = \alpha \cdot T_{e\_max}(\omega_e) \\ b_e = f_1(T_e, \omega_e) \\ P_e = T_e \cdot \omega_e \end{cases} \quad (1)$$

where  $T_e$  is the engine torque;  $\alpha$  is the throttle opening of the engine;  $\omega_e$  is the engine angular speed;  $b_e$  is the brake specific fuel consumption (BSFC) of the engine;  $f_1$  is the look-up table functions;  $P_e$  is the engine power.

This paper selects the WP6.180E40 diesel engine as the research object and gives the output torque, power, and BSFC curves of the engine at full throttle opening shown in Figure 3.

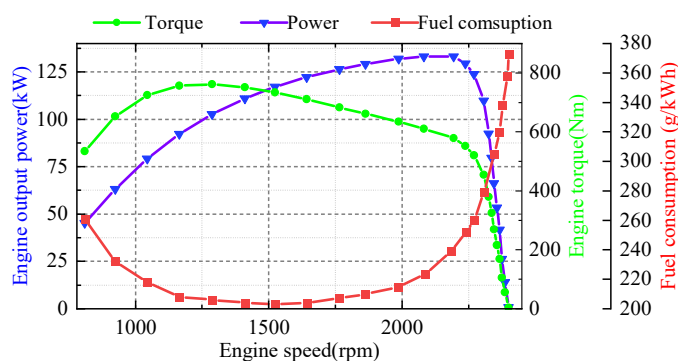


**Figure 3.** Full-load characteristics of the engine.

### 3.2. Motor Model

Ignoring the influence of motor thermodynamics, the static interpolation model of the motor can be established as follows [26]:

$$\begin{cases} T_m = \beta \cdot T_{m\_max}(\omega_m) \\ P_m = T_m \omega_m \eta_m^j \\ \eta_m = f^j(T_m, \omega_m) \end{cases} \quad (2)$$

where  $T_m$  is the motor torque;  $\beta$  is the motor torque load rate;  $P_m$  is the motor power;  $\eta_m$  is the motor efficiency;  $\omega_m$  is the motor angular speed;  $j$  is a parameter to judge the motor state, if  $j = 1$  the power is positive, it is a motor; if  $j = -1$  the power is negative, it is a generator;  $f^j$  is the motor efficiency interpolation function.

This paper selects the TZ205XS85K01 motor as the research object and gives experimentally measured maximum rated output torque; maximum rated output power curves of the motor shown in Figure 4.

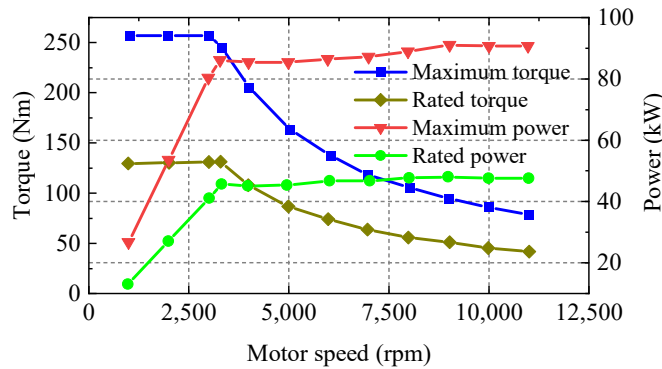


**Figure 4.** Toque and power characteristics of the motor.

### 3.3. Battery Model

The battery state of charge (SOC) is an important input signal for energy management and can be calculated as follows [27]:

$$\begin{cases} SOC_t = 1 - \frac{\int_0^t I_b dt}{Q_b} \\ I_b = \frac{V_{oc} - \sqrt{V_{oc}^2 - 4r_b P_b}}{2r_b} \end{cases} \quad (3)$$

where  $Q_b$  is the rated capacity of the battery;  $I_b$  is the charge and discharge current of the battery;  $V_{oc}$  is the open-circuit voltage of the battery;  $r_b$  is the internal resistance of the battery;  $P_b$  is the charge and discharge power of the battery.

The voltage and internal resistance of the battery can be expressed as:

$$\begin{cases} V_b = V_{oc} - r_b I_b \\ V_{oc} = f_{voc}(SOC) \\ r_b = f_{int}(SOC) \end{cases} \quad (4)$$

where  $f_{voc}$  and  $f_{int}$  are the look-up table functions of battery open-circuit voltage and battery internal resistance, respectively.

The internal resistance and the open-circuit voltage of the NiMH battery connected in series about SOC curves are shown in Figure 5.

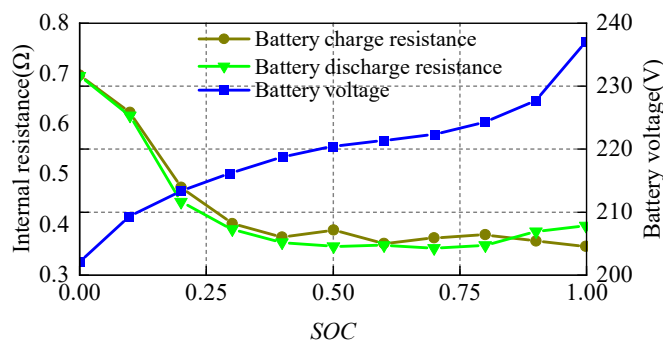


**Figure 5.** Battery parameters.

### 3.4. Transmission Model

As shown in Figure 6, there are three different power flow types of the HMT, and its efficiency depends on factors such as mechanical and volumetric efficiency, pressure, displacement angle, etc. Which can theoretically be determined by  $P_{out} / P_{in}$  [28,29].

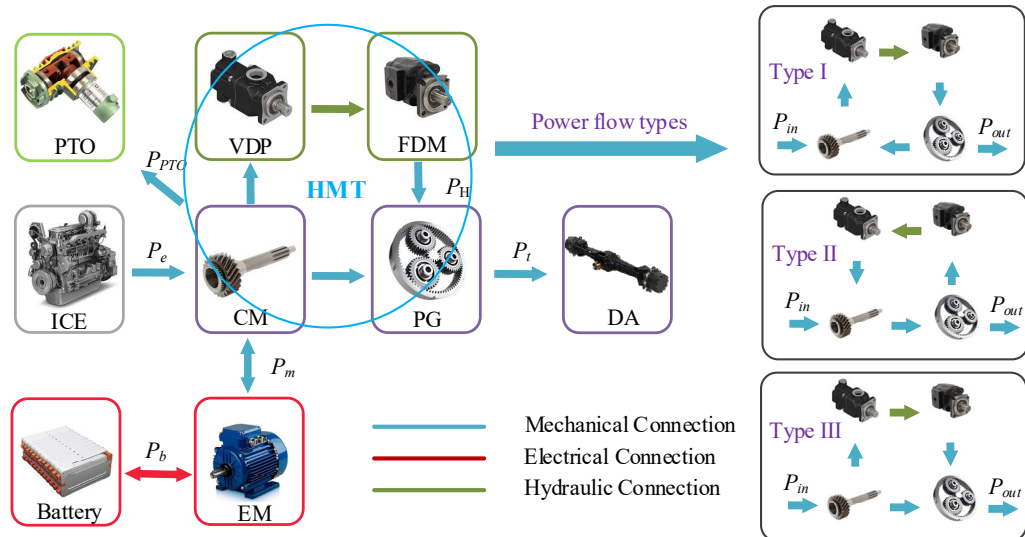


**Figure 6.** Power flow of powertrain system. (CM: coupling mechanism; ICE: internal combustion engine; VDP: variable displacement pump; FDM: fixed displacement motor; DA: drive axle;  $P_{PTO}$ : power take-off power;  $P_H$ : hydraulic system power;  $P_t$ : traction power.).

According to Figure 6: in type I power flow, the power of the hydraulic path is greater than the input power, and the HMT efficiency of this transmission mode is low because a large amount of power is transmitted through the inefficient hydraulic path; in type II power flow, the power of the hydraulic path is transmitted in the reverse direction, resulting in an increased power of the mechanical path, and the HMT efficiency of this mode is higher than type I and lower than type III; in type III power flow, the power is divided into hydraulic and mechanical paths and then merged, the power of both paths is transmitted in the positive direction, and the HMT efficiency in this mode is the highest.

$$\left\{ \begin{array}{l} \text{Type I : } \eta_{HMT} = \eta_M \left( 1 - \frac{P_H}{P_{in}} \right) + \eta_H^{-1} \left( \frac{P_H}{P_{in}} \right); \frac{P_H}{P_{in}} < 0 \\ \text{Type II : } \eta_{HMT} = \eta_M^{-1} \left( 1 - \frac{P_H}{P_{in}} \right) + \eta_H \left( \frac{P_H}{P_{in}} \right); \frac{P_H}{P_{in}} > 1 \\ \text{Type III : } \eta_{HMT} = \eta_M \left( 1 - \frac{P_H}{P_{in}} \right) + \eta_H \left( \frac{P_H}{P_{in}} \right); 0 < \frac{P_H}{P_{in}} < 1 \end{array} \right. \quad (5)$$

where  $\eta_{HMT}$  is the efficiency of hydro-mechanical transmission,  $\eta_M$  is the mechanical efficiency of the hydraulic components;  $\eta_H$  is the total efficiency of the hydraulic system. The efficiency of hydraulic components is varied under different test environments, Figure 7

gives the relevant efficiency curves of the SAUER\_DANFOSS 90-series hydraulic components measured experimentally at different pressures.

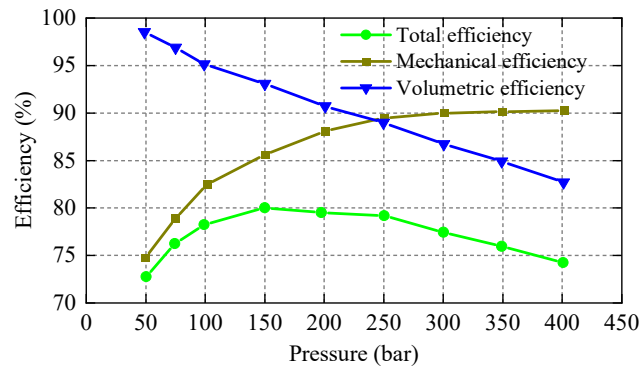


**Figure 7.** Efficiency characteristics of the hydraulic components.

The powertrain system efficiency of the tractor in each operating condition can be obtained by analyzing the power flow of power components in different operations. The system efficiency is:

$$\left\{ \begin{array}{l} \eta_s = \frac{P_i + P_{PTO} + (1-\tau)P_b}{P_e/\eta_e + \tau P_b} \\ \tau = \begin{cases} 0 & P_b \leq 0 \\ 1 & P_b > 0 \end{cases} \end{array} \right. \quad (6)$$

where  $\eta_e$  is the efficiency of the engine;  $\tau$  is a parameter to judge the battery state of charging or discharging; if the battery is in the charge state  $\tau = 0$ ; if the battery is in the discharge state  $\tau = 1$ .

### 3.5. Tractor Model

The longitudinal dynamics of the tractor [30] can be expressed as:

$$\left\{ \begin{array}{l} T_t i_g i_0 \eta_t - T_w = J_w \alpha_w \\ T_w = (F_T + \frac{1}{2} \rho C_D A v_a^2 + mg f \cos \theta + mg \sin \theta) r_w \\ v_a = \omega_w r_w / (1 + \delta) = \omega_{in} r_w / i_g i_0 (1 + \delta) \end{array} \right. \quad (7)$$

where  $T_t$  is the input torque of the traction mechanism;  $i_0$  is the transmission ratio of the drive axle;  $\eta_t$  is the transmission efficiency;  $T_w$  is the torque of the driving wheel;  $J_w$  is the equivalent moment inertia of the driving wheel;  $\alpha_w$  is the angular acceleration of the driving wheel;  $F_T$  is the hook tension;  $\rho$  is the mass density of air;  $C_D$  is the air resistance coefficient;  $v_a$  is the actual speed of the tractor;  $A$  is the frontal area of the tractor;  $m$  is the mass of the tractor;  $g$  is the gravity acceleration;  $f$  is the rolling resistance coefficient;  $\theta$  is the ramp angle;  $r_w$  is the radius of the driving wheel;  $\omega_w$  is the angular speed of driving wheel;  $\delta$  is the slip rate of the driving wheel;  $\omega_{in}$  is the angular speed of the input shaft.

## 4. Tractor Control Strategy

The tractor equipped with MEH-PS has a variety of driving modes and transmission modes, according to the tractor's requirement for power and speed in different operating conditions, and a reasonable choice of driving mode and transmission mode to maximize its performance. When using multiple power sources, drive also needs to consider the power distribution between power sources to achieve the optimal system efficiency.

### 4.1. Overall Control Strategy

The overall control strategy architecture of the tractor is shown in Figure 8. Firstly, the power demand of the tractor is determined based on the current tractor speed and the target speed of the driver as well as the real-time load of the tractor, then the optimal economy driving mode is selected according to the real-time battery SOC, and according to the

tractor's current mode to consider whether to switch the mode. The most suitable driving mode is selected between pure electric drive, pure engine drive, torque coupling drive, and speed coupling drive. Finally, the appropriate transmission mode is selected between hydrostatic transmission, hydro-mechanical transmission, and mechanical transmission to meet the optimal power transmission.

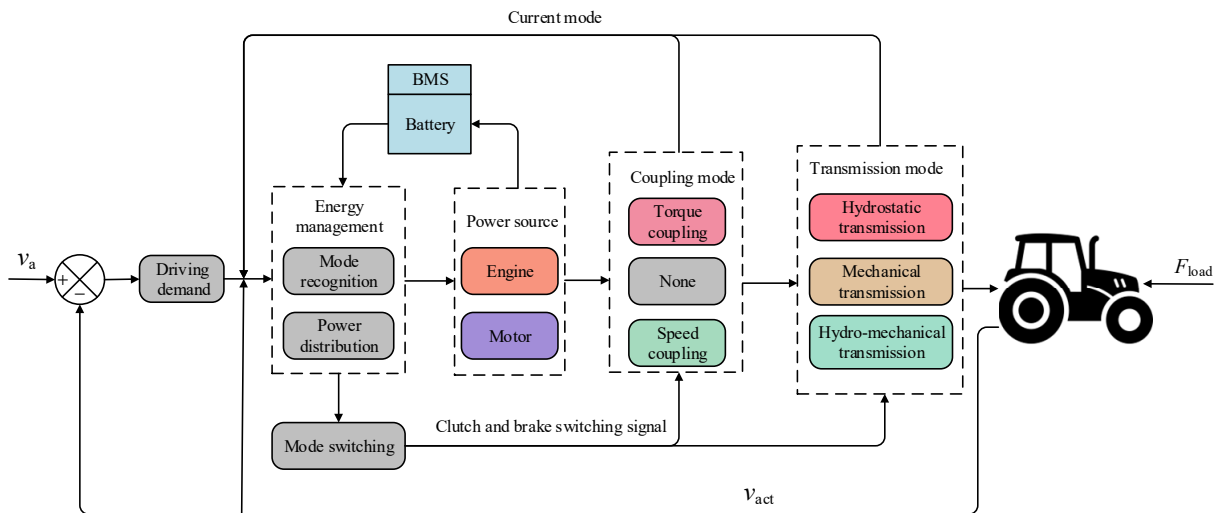


**Figure 8.** Tractor overall control architecture.

The matching of driving and transmission mode is developed according to the operating characteristics of the power source and transmission mode. For example, if the pure electric drive mode is selected, because the motor speed and torque can be freely adjusted in a wide range, there is no need to select the hydrostatic transmission or hydro-mechanical transmission while the mechanical transmission with the highest transmission efficiency can meet the transmission requirement and achieve stepless transmission [31].

#### 4.2. HMT Transmission Ratio Control Strategy

The transmission ratio of HMT should enable the engine to work on the optimal curve and meet the requirement of tractor speed [32]. Taking the optimal economy as an example, the relationship between the tractor speed and the engine speed is as follows:

$$i_g = \frac{2\pi n_{e\_opt} r_w}{60 i_0 v_a (1 + \delta)} \quad (8)$$

where  $n_{e\_opt}$  is the optimal economic speed of the current throttle opening of the engine, which can be obtained by calibration of an experimental test bench. For the diesel engine (WP6.180E40) selected in this paper, the fitting curve between  $n_{e\_opt}$  and  $\alpha$  is:

$$n_{e\_opt} = -210\alpha^4 - 150\alpha^3 + 810\alpha^2 + 1000\alpha + 750 \quad (9)$$

According to the above relationship, the HMT optimal economic transmission ratio map of the engine driving mode is shown in Figure 9.

#### 4.3. Mode Division of Rule-Based

A generally applicable rule-based pattern recognition strategy, as shown in Figure 10, was applied to classify the tractor in each power range to achieve the optimal performance of a tractor equipped with MEH-PS [33].

In the figure  $T_{opt}$  is the optimal engine torque;  $T_1$  is the maximum torque of pure electric drive mode;  $T_2$  is the maximum torque of driving charging;  $T_3$  is the maximum torque of pure engine drive mode;  $T_4$  is the maximum torque of speed coupling drive;  $n_{e\_max}$  is the rated speed of engine;  $SOC_h$  is the higher limit of the SOC efficient region;

$SOC_l$  is the lower limit of the SOC efficient region;  $v_{sta1}$  is the start completion speed of start type 1;  $v_{sta2}$  is the start completion speed of start type 2;  $i_{g\_min}$  is the minimum transmission ratio of HMT;  $s$  is the equivalence factor.

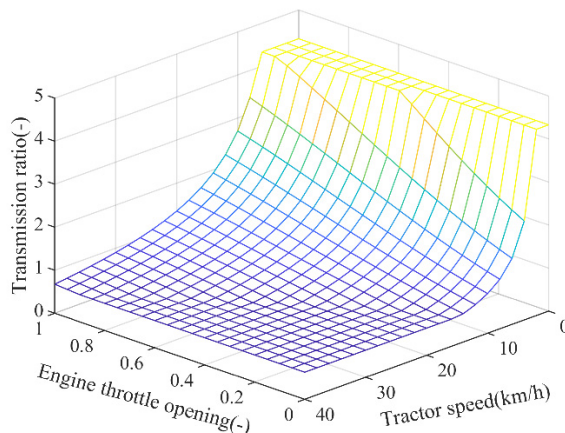


**Figure 9.** Map of HMT economic transmission ratio.

The initialization input parameters include  $SOC$ ,  $i_g$ ,  $T_{req}$ , and  $v$ . Firstly, whether the tractor needs to start is judged, and if so, determine the start type according to the required torque; for example, if the tractor is in the ploughing or transport or other starting conditions that require it to provide a large torque, the starting type (1) can be selected; if the tractor is in the transit condition, the required torque is small and  $SOC$  is sufficient, the starting type (2) can be selected. After the tractor reaches the start completion speed that is to switch to the operating mode, when the transmission mode is mechanical transmission, if stepless speed change is required then only the pure electric drive mode can meet the requirements, otherwise stepless speed change can be achieved through the engine-driven hydro-mechanical transmission.

Whether  $i_g < i_{g\_min}$  reflects the tractor's requirement for higher input speed. If so, the required speed is greater than the rated engine speed and  $SOC$  is high, it can be switched to the speed coupling drive mode to meet the requirement of higher speed; if  $SOC$  is low, the tractor can only be driven by the engine. If  $i_g \geq i_{g\_min}$ , the tractor's speed requirement is lower, according to the required torque, and  $SOC$  can choose the most appropriate driving mode in turn: pure electric drive, pure engine drive, torque coupling driving charging, and torque coupling motor assist.

#### 4.4. Optimization Strategy with Minimal Equivalent Fuel Consumption

The first step of energy management is to select the appropriate driving mode according to the currently required torque. If a single power source drive is selected, the power output is performed directly without power distribution. If dual power sources are selected, taking torque coupling as an example, torque is distributed to the engine and motor in the way that consumes the least amount of fuel according to the required torque.

The equivalence factor ( $s$ ) can equate the power consumption of the battery with the fuel consumption of the engine and calculate the power distribution combination corresponding to the lowest fuel consumption of the engine and the motor at any moment. The equivalence factor reflects the tendency of energy use, if  $s$  is large there will be a preference for using fuel and more power output from the engine; if  $s$  is small there will be a preference for using electricity and more power output from the motor [34]. Considering the  $SOC$  and energy distribution strategy, fuel consumption is saved through motor-driven if  $SOC$  is high; lower  $SOC$  is avoided through engine-driven if  $SOC$  is low. The special relationship between the equivalence factor and  $SOC$  can achieve the best power distribution between power sources and ensure the  $SOC$  within the high-efficiency

region [35]. The above analysis obtains the relationship between SOC, equivalence factor, and power distribution shown in Figure 11.

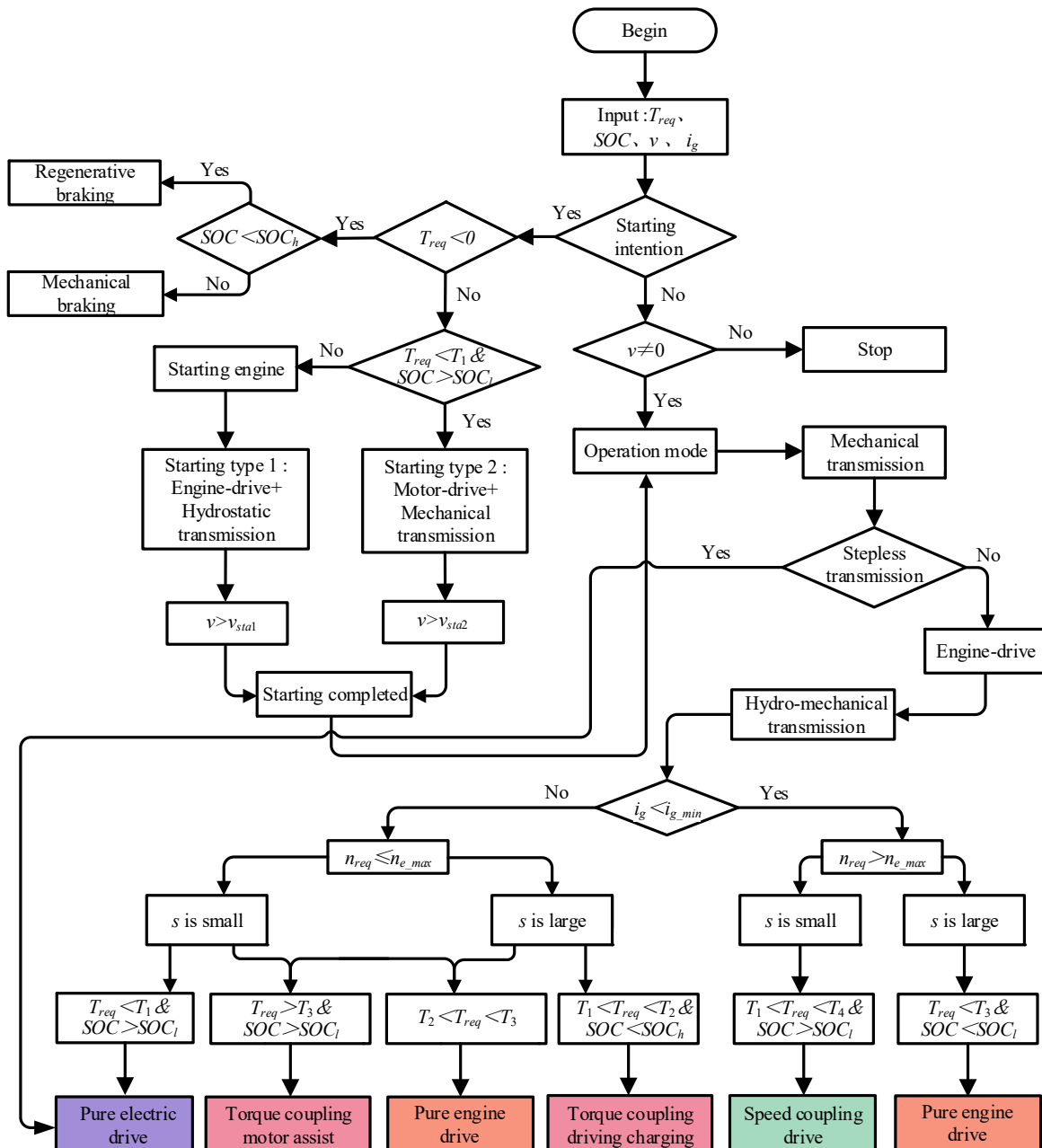


**Figure 10.** Rule-based MEH-PS workflow diagram.

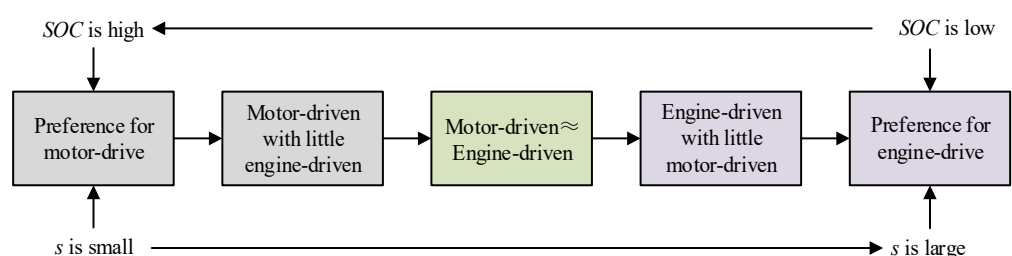


**Figure 11.** Logical relationships of equivalence factor and SOC.

The mathematical model [36] of equivalent fuel consumption is:

$$\begin{cases} \dot{m}_{eq} = \dot{m}_e + \dot{m}_b \\ m_e = \frac{P_e}{\eta_e Q_l} \\ m_b = \frac{s(t)}{\eta_b Q_l} P_b \end{cases} \quad (10)$$

where  $m_e$  is the engine fuel consumption;  $m_b$  is the battery equivalent fuel consumption;  $\eta_b$  is the charging or discharging efficiency of the battery;  $Q_l$  is the lower heating value of the fuel,  $s(t)$  is the equivalence factor which can be calculated by the following equation [37]:

$$\begin{cases} s(t) = s_0 + \Delta s \\ \Delta s = \varepsilon \frac{\Delta SOC}{SOC_h - SOC_l} \\ \Delta SOC = SOC_h - SOC(t) \\ \varepsilon = s_h - s_l \\ s_0 = s_l \end{cases} \quad (11)$$

where  $s_0$  is the initial value of the equivalence factor;  $\Delta s$  is the change of the equivalence factor;  $\Delta SOC$  is the change of  $SOC$ ;  $s_h$  is the higher limit of the equivalence factor;  $s_l$  is the lower limit of the equivalence factor;  $\varepsilon$  is the  $SOC$  penalty factor.

According to the principle of Pontryagin minimization, the optimal output torque can be calculated from Equations (13)–(15) by the objective function  $J$ .

$$\begin{cases} \min_{u \in U} \left\{ J(u) = \int_0^T L(x(t), u(t), t) dt \right\} \\ H(u(t), x(t), t) = L(x(t), u(t), t) + p(t) \dot{x}(t) \end{cases} \quad (12)$$

where  $J$  is the objective function;  $L$  is the instantaneous fuel consumption;  $u$  is the distribution of energy between the engine and motor;  $H$  is the Hamiltonian function,  $x(t)$  is the  $SOC$ ;  $p(t)$  is the co-state variable of the system.

The minimum fuel consumption can be reached by:

$$\frac{\partial H}{\partial u} = \frac{\partial L}{\partial u} + p \frac{\partial f}{\partial u} = 0 \quad (13)$$

where  $f$  is the function controlling variations of state of charge of the battery.

The optimal command  $u_{opt}$  can be obtained by Equation (14), and obtain  $T_m^{opt}$  and  $T_e^{opt}$  by:

$$\begin{cases} u_{opt}(t) = T_m^{opt}(t) = \operatorname{argmin}\{H(u(t), x(t), t)\} \\ T_{req}(t) = T_m^{opt}(t) + T_e^{opt}(t) \end{cases} \quad (14)$$

where  $T_m^{opt}$  and  $T_e^{opt}$  is the optimal torque of the motor and engine.

The multiple constraints given by the system's components engine, motor, and the battery is as follows:

$$\begin{cases} T_e \in [0, T_{e,max}(\omega_e)] \\ \omega_e \in [\omega_{e,min}, \omega_{e,max}] \\ T_m \in [T_{m,min}(\omega_m), T_{m,max}(\omega_m)] \\ \omega_m \in [\omega_{m,min}, \omega_{m,max}] \\ SOC \in [SOC_{min}, SOC_{max}] \end{cases} \quad (15)$$

Taking the motor torque as the control variable, the equivalent fuel consumption of all possible combinations of engine and motor torque is calculated according to a certain iterative gradient when the required torque is determined [38], and the combination of the lowest fuel consumption is taken as the optimal power distribution scheme, the calculation flow is shown in Figure 12.

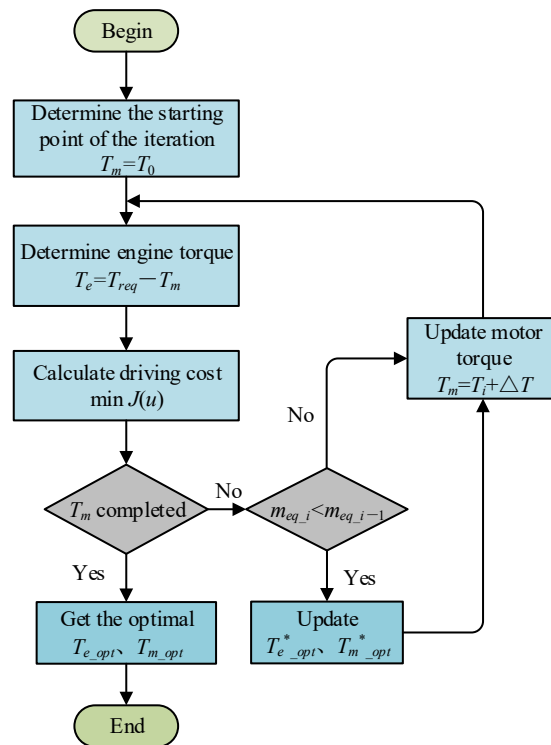


**Figure 12.** Flowchart of procedure for optimal torque.

## 5. Simulation and Experiment

### 5.1. Simulation Modeling

A tractor model equipped with the MEH-PS shown in Figure 13 was established in SimulationX. The performance of the powertrain can be evaluated through simulation. With the help of the component library of SimulationX, the engine model, motor model, transmission model, chassis model, mode switching unit, transmission ratio calculation unit, and power distribution unit are created using the cross-domain equation-based concept of the Modelica language. The tractor simulation parameters are shown in Table A1 (see Appendix A).

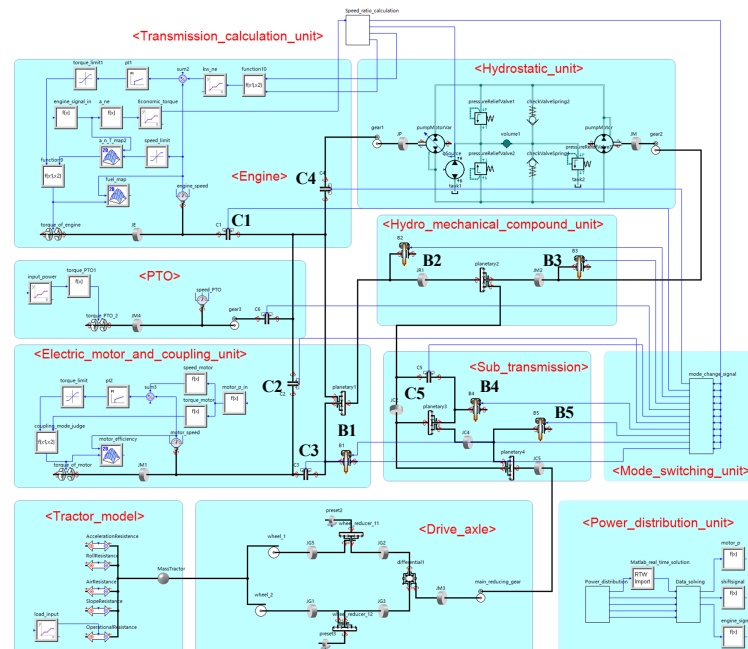


**Figure 13.** A tractor simulation model based on SimulationX.

### 5.2. Test Bench and Principle

The test bench illustrated in Figure 14 was established to verify the performance of a tractor equipped with a MEH-PS, which is based on the AVL dynamometer. The overall test scheme architecture of the test bench is shown in Figure 15. The main control computer of the test bench communicates with the HCU (hybrid controller unit) to realize observation and calibration. The HCU indirectly communicates with the variable frequency drive and control system, the battery, and the dynamometer power cabinet through the data acquisition and exchange system. The motor is directly controlled by the motor controller. The HMT displacement ratio is controlled by the DSP (digital signal processing) controller. The clutches and brakes are indirectly controlled by the PWM (pulse width modulation) voltage amplifier and electromagnetic reversing valve to complete the mode switching.



**Figure 14.** Test bench: 1. Oil cooling system; 2. motor cooling system; 3. variable frequency motor; 4. driving motor and coupling mechanism; 5. HMT; 6. central transmission device; 7. power cabinet of dynamometer; 8. electrical dynamometer; 9. data acquisition cabinet.

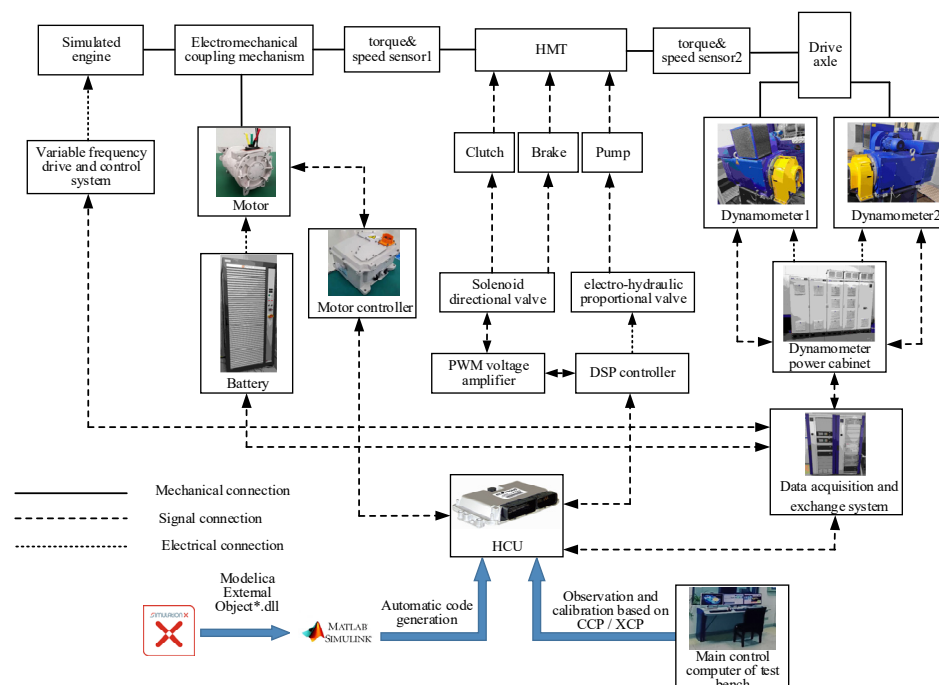


**Figure 15.** Test bench architecture scheme.

### 5.3. Simulation and Test of Tractor Operation

#### 5.3.1. Ploughing Analysis

Ploughing is the main task of the tractor, the pulling force [39] of the plough on the tractor's hook is:

$$F_T = F_G f + (\lambda + \kappa v^2) abn \quad (16)$$

where  $F_G$  is the weight of the plough;  $\lambda$  is the soil specific resistance;  $\kappa$  is the relevant coefficient of plough surface and soil;  $a$  is the ploughing depth;  $b$  is the ploughing width;  $n$  is the number of ploughs. The plough in this study is a six-share turning plough (1LF-550) with dimensions of  $5200 \times 2600 \times 1850$  mm ( $L \times W \times H$ ) and a mass of 1800 kg.

Tractors do not have a specific driving cycle, therefore speed and tension sensors are used to collect data of driving speed and traction resistance, which are important input conditions for the cycle [40]. The actual ploughing is affected by soil properties, and the change of ploughing resistance is random. The relevant conditions of the actual measurement process are shown in Table 4. Take the traction resistance shown in Figure 16 as the input resistance, and the measured tractor speed shown in Table 4 is adopted as the target tractor speed during ploughing operation.

**Table 4.** Measurement conditions of ploughing resistance.

Time (s)	Tractor Speed (km/h)	Ploughing Depth (m)
0~100	9.00	0.10
100~200	9.00	0.18
200~300	9.00	0.26
300~400	7.00	0.34

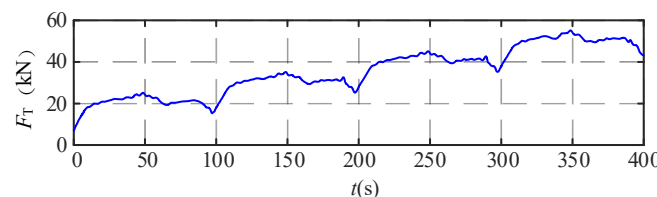


**Figure 16.** Ploughing cycle.

Figure 17 shows the results of the ploughing operation. Although the ploughing resistance keeps changing, the tractor speed remains constant. Due to the large starting torque, the starting type 1 is selected at 0~5 s. At 10~100 s the tillage depth is small, and the required torque is small, the excess torque is used for power generation so that the engine operating point is transferred to a higher load. After 100 s, the tractor works in the pure engine drive mode, HMT can adjust the transmission ratio according to the driving force required for ploughing so that the engine operating points are distributed in the lower fuel consumption region, and the BSFC is maintained in the range of 205~211 g/(kW·h). The instant fuel consumption is between 11~31 L/h, and the overall fuel consumption of the tractor is relatively low. In the ploughing process, the HMT efficiency under different loads is between 0.84~0.9, and the system efficiency is between 0.34~0.37. The above results show that the whole ploughing operation has a good fuel consumption performance under different ploughing resistance.

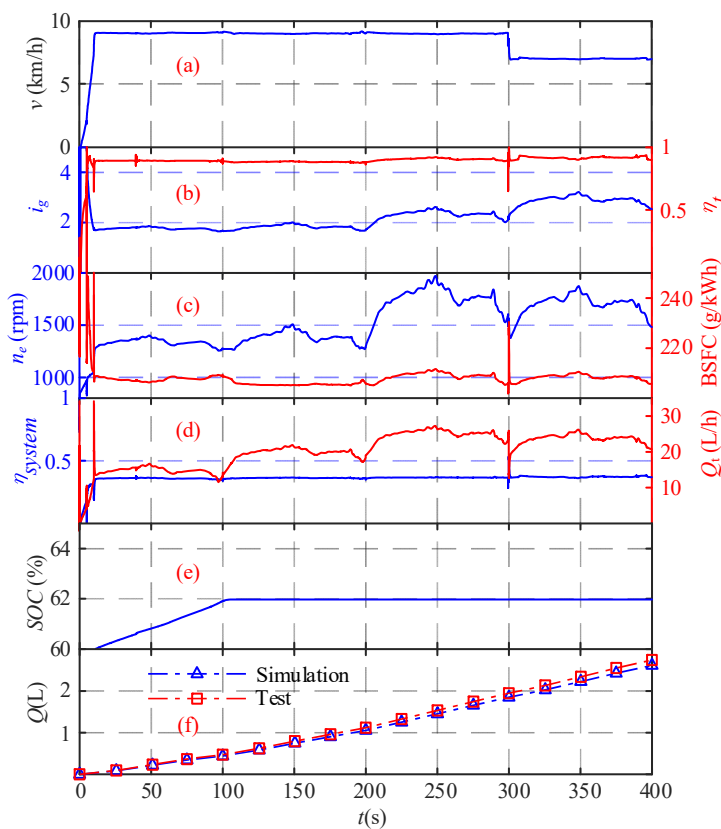


**Figure 17.** Results of the ploughing operation: (a) tractor speed, (b) transmission ratio and efficiency, (c) engine speed and BSFC, (d) system efficiency and instant fuel consumption, (e) SOC curve, (f) simulation and test fuel consumption.

### 5.3.2. Harvest Analysis

Taking the data measured during the harvest operation as input condition, the tractor driving force, target tractor speed, and PTO required power are shown in Figure 18.

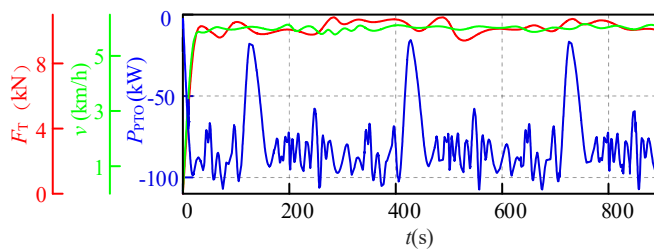


**Figure 18.** Harvest cycle.

Figure 19 shows the harvest operation results: tractor speed and target speed are consistent, engine speed and transmission ratio are nearly unchanged, and the tractor operates in the torque coupling mode. The required power in the harvest operation mainly comes from the PTO, and the required power from the walking mechanism is relatively small. Under the regulation of the equivalent fuel consumption minimization control strategy, the motor torque is changed according to the required torque of the walking mechanism and the PTO, so that the system can obtain the highest efficiency. In addition, the motor torque regulation keeps the engine speed smooth and provides a stable output speed for the PTO to drive other mechanisms. The BSFC during harvest operation is kept in the range of 206~211 g/(kW·h), and the instant fuel consumption is between 10.4~32.3 L/h. The efficiency of HMT is kept above 0.89, and the system efficiency is kept above 0.39. The above results show that the energy management strategy developed for this

powertrain system can meet both the PTO and walking mechanism power requirements while maintaining high tractor system efficiency.

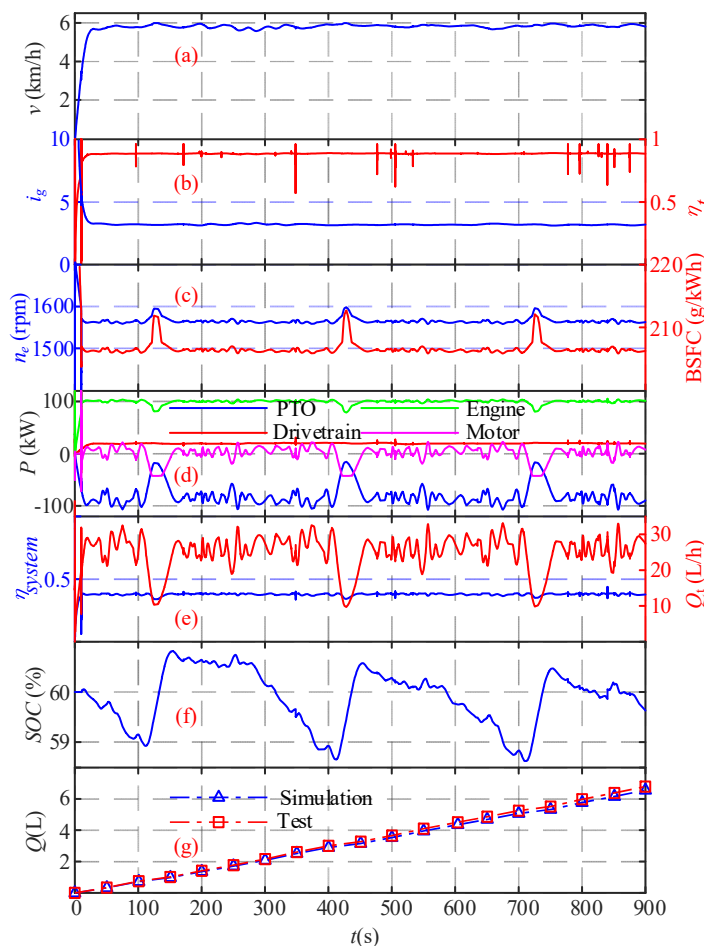


**Figure 19.** Results of the harvest operation: (a) tractor speed, (b) transmission ratio and efficiency, (c) engine speed and BSFC, (d) power of related components, (e) system efficiency and instant fuel consumption, (f) SOC curve, (g) simulation and test fuel consumption.

### 5.3.3. Transport Analysis

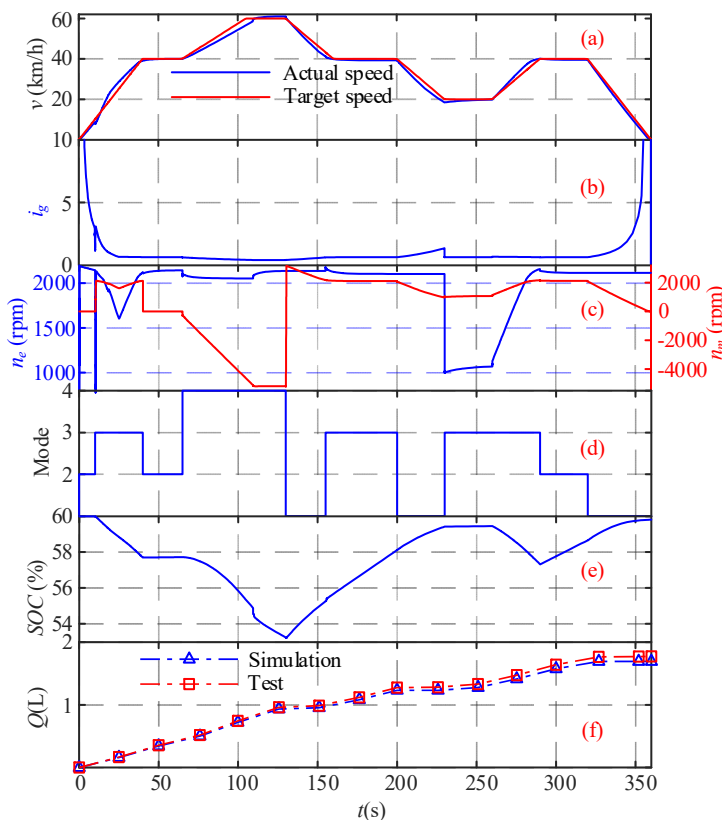
The tractor is subjected to the traction force from the trailer during transport operation. If the connection between the tractor and the trailer is rigid, they will share the same longitudinal speed. The longitudinal force of the tractor is:

$$F_t = m_t g \sin \theta + m_t g f \cos \theta + m_t \frac{dv_a}{dt} + \frac{C_D A v_a^2}{21.15} \quad (17)$$

where  $m_t$  is the total mass of the tractor and trailer, this paper takes full load transport as the research objective, the mass of the trailer is 5010 kg, the mass of the cargo is 13,080 kg, and the total mass of the tractor is 26,350 kg.

Figure 20 shows transport operation results: the tractor starts with starting type 1 at 0~10 s, then switches to the torque coupling motor assist mode at 10~40 s, the tractor has greater acceleration. When the tractor speed is greater than 40 km/h, it switches to the speed coupling mode, and the tractor speed increases with the increase of the motor speed until 60 km/h. Tractor acceleration is relatively slow in this process, which is the difference between speed coupling and torque coupling, but the maximum speed of the tractor is improved, and the transport efficiency is higher. The engine is kept at a higher speed, and the transmission ratio is kept near during transport operation. There are many

modes in this process, as shown in Table 1 for the corresponding relationship of each mode in Figure 20d.



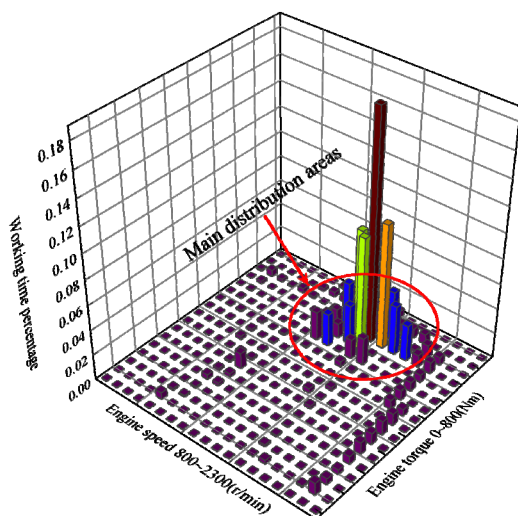
**Figure 20.** Results of the transport operation: (a) tractor speed, (b) transmission ratio, (c) engine and motor speed (d) driving mode, (e) SOC curve, (f) simulation and test fuel consumption.

Table 5 summarizes the SOC and fuel consumption data of the three operations discussed above. The SOC initial and end differences are small, the battery charge and discharge are generally balanced, and the tractor external energy comes mainly from the engine. The simulation data are reliable because the fuel consumption of the test value and the simulation of the maximum error does not exceed 5%.

**Table 5.** Summary of SOC and fuel consumption.

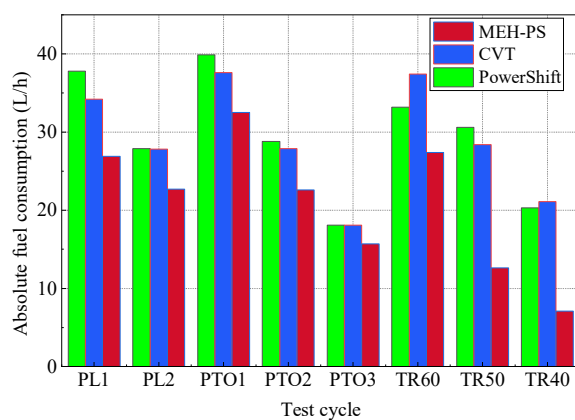
Parameter	Ploughing	Harvest	Transport
SOC initial value/final value (%)	60.00/61.96	60.00/59.63	60.00/59.81
SOC difference (%)	+1.96	-0.37	-0.19
Simulation/test fuel consumption (L)	2.59/2.72	6.56/6.80	1.69/1.77
Fuel consumption error (%)	4.8	3.5	4.5

Figure 21 shows the distribution of engine operating points under the above three operations. It can be seen from the figure that the developed hybrid system energy management strategy cooperates with the stepless speed change function of HMT, the engine operating points are mainly distributed in the area of higher load, and the engine operating in this area has lower fuel consumption and higher efficiency.



**Figure 21.** Engine working time percentage distribution.

To make the data more comparable, the fuel consumption of the CLAAS AXION 850 Hexashift, a tractor with PowerShift transmission of nearly similar horsepower, and the Fendt 724 Vario SCR, a tractor with the continuously variable transmission, were compared according to the standard test cycle for tractors published by the Deutsche Landwirtschafts-Gesellschaft (DLG). The test cycle consists of 14 operating conditions and is performed on the PowerMix according to the relevant requirements of the OECD Code2 to simulate the tractor in typical operating and transport conditions and to measure the fuel consumption, output power, and efficiency during the cycle. Figure 22 shows the comparison of fuel consumption under different test conditions for the ploughing condition (PL), the power take-off operation (PTO), and the transport operation (TR). The specific values are shown in Table A2. From the figure, it can be seen that the tractor has the lowest fuel consumption for MEH-PS in field and transport operations compared with PowerShift and CVT.



**Figure 22.** Fuel consumption of tractors equipped with different transmissions in different test cycles.

Since the indicators to measure the fuel consumption of the tractor in different operations are different, to compare the fuel consumption obtained from the above conditions more intuitively the test results were further processed to obtain the average fuel consumption of the tractor equipped with the above transmission in field operations, PTO operations, and transport operations as shown in Figure 23.

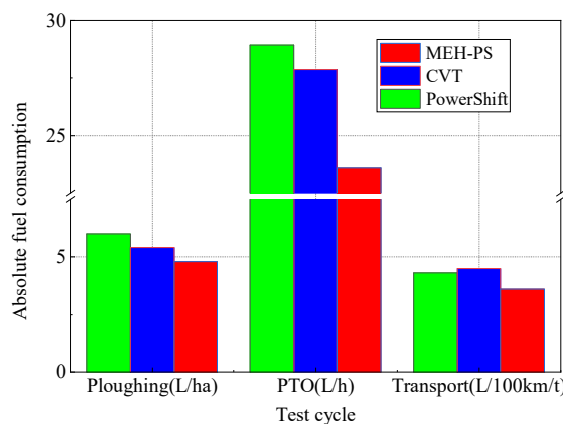


**Figure 23.** Comparison of fuel consumption of tractors equipped with different transmissions.

Comparing the results above, it was found that the transmission scheme proposed in this paper is 20% more fuel-efficient than PowerShift tractors under ploughing conditions and 9% more fuel-efficient than CVT tractors; 18% more fuel-efficient than PowerShift tractors, and 15% more fuel-efficient than CVT tractors under power output conditions; 15% more fuel-efficient than PowerShift tractors and 19% more fuel-efficient than CVT tractors under transport conditions. The above results further demonstrate the reliable fuel-saving capability of the proposed scheme and the developed energy management strategy in this paper.

## 6. Discussion

In this paper, a new mechanic-electronic-hydraulic powertrain system has been designed to solve the problems encountered in hydro-mechanical transmissions and hybrid tractors with the following main efforts.

1. In terms of structural design, compared to a typical hydro-mechanical transmission, this paper uses only a single planetary row for the merging of the hydraulic and mechanical power, which has fewer planetary gears compared to the structure mentioned in the paper [41]. Moreover, the advantages of hybrid power can be exploited without the need for more powerful electrical equipment.
2. The speed ratio control strategy and energy management strategy are designed for the hybrid tractor, and three tractor operating conditions of the whole tractor is simulated. Moreira pointed out that there are no standard test conditions for hybrid tractors, however, the data from the actual tractor operation is reliable and can be a reference for the research of hybrid tractors [42].
3. The feasibility of the MEH-PS scheme was confirmed by comparing the difference between bench test and simulation data within 5% and comparing the fuel consumption of PowerShift tractors and CVT tractors published by DLG under the corresponding operating conditions. It was found that the device has the lowest fuel consumption, which further confirms the reliability of the scheme, and the scheme has practical value for energy saving of agricultural machinery.

## 7. Conclusions

This paper designs a MEH-PS based on the actual requirements of the tractor. The principle of drive and transmission implementation of the powertrain system is introduced, and the HMT transmission ratio control strategy and hybrid system energy management strategy are developed.

The ploughing, harvest, and transport operations are analyzed. Ploughing operation is mainly works in the pure engine drive mode, HMT can continuously change the transmission ratio according to the ploughing resistance so that the engine operates in the lower fuel consumption region while the transmission also has high efficiency to reduce

tractor fuel consumption. Harvesting operation mainly works in the torque coupling drive mode, which can reasonably allocate the power source to perform work according to the developed rule-based optimization energy management strategy to meet the power requirements of the walking mechanism and PTO. Transport operation can gain more driving force, broaden the tractor speed range, minimize fuel consumption, and improve transport efficiency by a variety of driven modes.

The simulation and test fuel consumption error of the three operations are within 5% and is lower than the fuel consumption of similar horsepower PowerShift and CVT tractors published by DLG. The developed hybrid system energy management strategy and HMT transmission ratio control strategy can achieve energy saving results. The powertrain system provides a solution for modern agriculture to reduce tractor energy consumption under multiple operations.

## 8. Patents

The mechanic-electronic-hydraulic powertrain system reported in this manuscript has been authorized in China (Authorization No. CN 112128336 B, Patent No. ZL 2020 1 0766107.2).

**Author Contributions:** Conceptualization, Z.Z. and D.W.; methodology, Z.Z.; software, L.L.; experiment, D.W. and Y.Y.; data collation, L.L. and Y.Y.; funding acquisition, Y.C. and Z.Z.; supervision, Y.C. and L.L.; writing-original draft, L.L. and Z.Z. All authors have read and agreed to the published version of the manuscript.

**Funding:** This work was supported in part by the Project of State Key Laboratory of Power System of Tractor under Grant SKT2022011 and in part by the National Natural Science Foundation of China under Grant 51805222, Grant 51875255, Grant U20A20331, and in part by the Project of Jiangsu Provincial Six Talent Peaks under Grant 2018-TD-GDZB-022.

**Institutional Review Board Statement:** Not applicable.

**Informed Consent Statement:** Not applicable.

**Data Availability Statement:** The data presented in this study are available on request from the corresponding author at (2211904012@stmail.ujs.edu.cn).

**Conflicts of Interest:** The authors declared no potential conflict of interest.

## Appendix A

**Table A1.** Parameters of the tractor and key components.

Item	Parameter	Specification
Tractor	Mass	8260 kg
	Radius of wheels	750 mm
Engine	Rated power	132 kW@2200 r/min
	Maximum torque	750 Nm@1300 r/min
	Minimum fuel consumption	203 g/kW·h@1500 r/min
Motor	Rated power	45 kW
	Rated speed	3300 r/min
	Maximum speed	11,000 r/min
Battery	Capacity	45 Ah
	Nominal voltage	360 V
Driveline	Transmission ratio	0.63~4.33
	Gear ratio of main reducer	6.4
	Gear ratio of wheel reducer	3.7

**Table A2.** Relevant data obtained from DLG test conditions.

Load Type	Test Cycle	Engine Speed (r/min)		Driving Speed (km/h)		Absolute Fuel Consumption (L/h)		BSFC (g/kWh)	
		PowerShiftCVT	MEH-PS	PowerShiftCVT	MEH-PS	PowerShiftCVT	MEH-PS	PowerShiftCVT	MEH-PS
Drawbar work	PL1	1407	1348	1684	7.1	6.7	7.0	37.8	26.9
	PL2	1312	1393	1407	8.5	8.8	9.1	27.9	22.7
Drawbar + PTO work	PTO1	1663	1622	1558	5.6	5.7	5.7	39.9	32.5
	PTO2	1424	1664	1567	5.5	5.9	5.8	28.8	22.6
	PTO3	1433	1684	1574	5.5	5.9	5.8	18.1	15.7
Transport work	TR60	1989	1448	2140	60.3	61.2	60.1	33.2	27.4
	TR50	1908	1201	2135	51.1	50.4	50.0	30.0	28.4
	TR40	1478	1015	2079	40.8	40.2	40.0	20.3	21.0
								573	580
								539	610
								266	643
									259
									266
									236
									207
									208
									205

## References

1. Data Query System of Ministry of Agriculture and Rural Affairs of the People's Republic of China. Available online: <http://zdsccxx.moa.gov.cn:8080/nyb/pc/search.jsp> (accessed on 26 February 2022).
2. The State Council on the Issuance of the “13th Five-Year Plan” Comprehensive Work Program of Energy Saving and Emission Reduction Notice. Available online: [http://www.gov.cn/zhengce/content/2017-01/05/content\\_5156789.htm#](http://www.gov.cn/zhengce/content/2017-01/05/content_5156789.htm#) (accessed on 5 January 2017).
3. Opinions on the Key Work of Comprehensive Promotion of Rural Revitalization in 2022. Available online: <https://xhpfmapi.xinhuaxtm.com/vh512/share/10614093> (accessed on 22 February 2022).
4. Scolaro, E.; Alberti, L.; Barater, D. Electric Drives for Hybrid Electric Agricultural Tractors. In Proceedings of the 2021 IEEE Workshop on Electrical Machines Design, Control and Diagnosis (WEMDCD), Modena, Italy, 8–9 April 2021; pp. 331–336.
5. Renius, K.T.; Resch, R. *Continuously Variable Tractor Transmissions*; American Society of Agricultural Engineers: St. Joseph, MI, USA, 2005.
6. Yu, J.; Cao, Z.; Cheng, M.; Pan, R. Hydro-mechanical power split transmissions: Progress evolution and future trends. *Proc. Inst. Mech. Eng. Part D J. Automob. Eng.* **2019**, *233*, 727–739. [[CrossRef](#)]
7. Xia, Y.; Sun, D.; Qin, D.; Zhou, X. Optimisation of the power-cycle hydro-mechanical parameters in a continuously variable transmission designed for agricultural tractors. *Biosyst. Eng.* **2020**, *193*, 12–24. [[CrossRef](#)]
8. Li, B.; Sun, D.; Hu, M.; Zhou, X.; Wang, D.; Xia, Y.; You, Y. Automatic gear-shifting strategy for fuel saving by tractors based on real-time identification of draught force characteristics. *Biosyst. Eng.* **2020**, *193*, 46–61. [[CrossRef](#)]
9. Wan, L.; Dai, H.; Zeng, Q.; Sun, Z.; Tian, M. Characteristic analysis and co-validation of hydro-mechanical continuously variable transmission based on the wheel loader. *Appl. Sci.* **2020**, *10*, 5900. [[CrossRef](#)]
10. Rossetti, A.; Macor, A. Control strategies for a powertrain with hydromechanical transmission. *Energy Procedia* **2018**, *148*, 978–985. [[CrossRef](#)]
11. Xiao, M.; Zhao, J.; Wang, Y.; Zhang, H.; Lu, Z.; Wei, W. Fuel economy of multiple conditions self-adaptive tractors with hydro-mechanical CVT. *Int. J. Agric. Biol. Eng.* **2018**, *11*, 102–109. [[CrossRef](#)]
12. Ahn, S.; Choi, J.; Kim, S.; Lee, J.; Choi, C.; Kim, H. Development of an integrated engine-hydro-mechanical transmission control algorithm for a tractor. *Adv. Mech. Eng.* **2015**, *7*, 1–18. [[CrossRef](#)]
13. Karner, J.; Baldinger, M.; Reichl, B. Prospects of hybrid systems on agricultural machinery. *GSTF J. Agric. Eng.* **2014**, *1*, 33–37. [[CrossRef](#)]
14. Delgado, O.; Lutsey, N. *Advanced Tractor-Trailer Efficiency Technology Potential in the 2020–2030 Timeframe*; The International Council on Clean Transportation: Washington, DC, USA, 2015; Report in preparation.
15. Mcfadzean, B.; Butters, L. An investigation into the feasibility of hybrid and all-electric agricultural machines. *Sci. Pap. Ser. A Agron* **2017**, *60*, 500–511.
16. Katrašnik, T. Energy conversion phenomena in plug-in hybrid-electric vehicles. *Energy Convers. Manag.* **2011**, *52*, 2637–2650. [[CrossRef](#)]
17. Guo, H.; Wang, X.; Li, L. State-of-charge-constraint-based energy management strategy of plug-in hybrid electric vehicle with bus route. *Energy Convers. Manag.* **2019**, *199*, 111972. [[CrossRef](#)]
18. Lee, D.; Kim, Y.; Choi, C.; Chung, S.; Inoue, E.; Okayasu, T. Development of a parallel hybrid system for agricultural tractors. *J. Fac. Agric. Kyushu Univ.* **2017**, *62*, 137–144. [[CrossRef](#)]
19. Kim, W.-S.; Kim, Y.-J.; Chung, S.-O.; Lee, D.-H.; Choi, C.-H.; Yoon, Y.-W. Development of simulation model for fuel efficiency of agricultural tractor. *Korean J. Agric. Sci.* **2016**, *43*, 116–126. [[CrossRef](#)]
20. Li, X.; Zhang, L.; Yang, S.; Liu, N. Analysis and experiment of HMT stationary shift control considering the effect of oil bulk modulus. *Adv. Mech. Eng.* **2020**, *12*, 1–13. [[CrossRef](#)]
21. Rossi, C.; Pontara, D.; Falcomer, C.; Bertoldi, M.; Mandrioli, R. A Hybrid-Electric Driveline for Agricultural Tractors Based on an e-CVT Power-Split Transmission. *Energies* **2021**, *14*, 6912. [[CrossRef](#)]

22. Zhu, Z.; Lai, L.; Sun, X.; Chen, L.; Cai, Y. Design and Analysis of a Novel Mechanic-Electronic-Hydraulic Powertrain System for Agriculture Tractors. *IEEE Access* **2021**, *9*, 153811–153823. [[CrossRef](#)]
23. Haughey, J.R.; Steward, B.L.; Ryan, S.J.; Kankamalage, R.G. Modeling Hybrid Hydro-Electro-Mechanical Power-Split Propulsion Systems. In Proceedings of the Fluid Power Systems Technology, Virtual, 19–21 October 2021; p. V001T001A047.
24. Cheng, Z.; Lu, Z.; Qian, J. A new non-geometric transmission parameter optimization design method for HMCVT based on improved GA and maximum transmission efficiency. *Comput. Electron. Agric.* **2019**, *167*, 105034. [[CrossRef](#)]
25. Hui, S.; Lifu, Y.; Junqing, J.; Yanling, L. Control strategy of hydraulic/electric synergy system in heavy hybrid vehicles. *Energy Convers. Manag.* **2011**, *52*, 668–674. [[CrossRef](#)]
26. Onori, S.; Serrao, L.; Rizzoni, G. *Hybrid Electric Vehicles: Energy Management Strategies*; Springer: London, UK, 2016.
27. Liu, T.; Tang, X.; Wang, H.; Yu, H.; Hu, X. Adaptive hierarchical energy management design for a plug-in hybrid electric vehicle. *IEEE Trans. Veh. Technol.* **2019**, *68*, 11513–11522. [[CrossRef](#)]
28. Ince, E.; Güler, M.A. Design and analysis of a novel power-split infinitely variable power transmission system. *J. Mech. Des.* **2019**, *141*, 054501. [[CrossRef](#)]
29. Manring, N.D. Mapping the efficiency for a hydrostatic transmission. *J. Dyn. Syst. Meas. Control.* **2016**, *138*, 031004. [[CrossRef](#)]
30. Renius, K.T. *Fundamentals of Tractor Design*; Springer: Cham, Switzerland, 2020.
31. Carl, B.; Ivantysynova, M.; Williams, K. *Comparison of Operational Characteristics in Power Split Continuously Variable Transmissions*; Sae technical paper; SAE: Warrendale, PA, USA, 2006; ISSN 0148-7191.
32. Chancellor, W.; Thai, N. Automatic control of tractor transmission ratio and engine speed. *Trans. ASAE* **1984**, *27*, 642–646. [[CrossRef](#)]
33. Hofman, T.; Steinbuch, M.; Van Druten, R.; Serrarens, A. Rule-based energy management strategies for hybrid vehicles. *Int. J. Electr. Hybrid Veh.* **2007**, *1*, 71–94. [[CrossRef](#)]
34. Gu, B.; Rizzoni, G. An adaptive algorithm for hybrid electric vehicle energy management based on driving pattern recognition. In Proceedings of the ASME International Mechanical Engineering Congress and Exposition, Chicago, IL, USA, 5–10 November 2006; pp. 249–258.
35. Zhang, L.; Liu, W.; Qi, B. Energy optimization of multi-mode coupling drive plug-in hybrid electric vehicles based on speed prediction. *Energy* **2020**, *206*, 118126. [[CrossRef](#)]
36. Wang, F.; Xia, J.; Xu, X.; Cai, Y.; Ni, S.; Que, H. Torsional vibration-considered energy management strategy for power-split hybrid electric vehicles. *J. Clean. Prod.* **2021**, *296*, 126399. [[CrossRef](#)]
37. Zhang, L.; Liu, W.; Qi, B. Innovation design and optimization management of a new drive system for plug-in hybrid electric vehicles. *Energy* **2019**, *186*, 115823. [[CrossRef](#)]
38. Gökce, K.; Ozdemir, A. An instantaneous optimization strategy based on efficiency maps for internal combustion engine/battery hybrid vehicles. *Energy Convers. Manag.* **2014**, *81*, 255–269. [[CrossRef](#)]
39. Xia, Y.; Sun, D.; Qin, D.; Hou, W. Study on the Design Method of a New Hydro-Mechanical Continuously Variable Transmission System. *IEEE Access* **2020**, *8*, 195411–195424. [[CrossRef](#)]
40. Han, J.; Xia, C.; Shang, G.; Gao, X. In-field experiment of electro-hydraulic tillage depth draft-position mixed control on tractor. In Proceedings of the IOP Conference Series: Materials Science and Engineering, Changsha, China, 28–29 October 2017; p. 012028.
41. Liu, F.; Wu, W.; Hu, J.; Yuan, S. Design of multi-range hydro-mechanical transmission using modular method. *Mech. Syst. Signal Processing* **2019**, *126*, 1–20. [[CrossRef](#)]
42. Moreda, G.; Muñoz-García, M.; Barreiro, P. High voltage electrification of tractor and agricultural machinery—A review. *Energy Convers. Manag.* **2016**, *115*, 117–131. [[CrossRef](#)]